

Utilizing of high-pressure high-temperature synthesis to enhance the thermoelectric properties of $Zn_{0.98}Al_{0.02}O$ with excellent electrical properties

Qi Chen(陈启), Xinjian Li(李欣健), Yao Wang(王遥), Lijie Chang(常立杰), Jian Wang(王健), Yuewen Zhang(张跃文), Hongan Ma(马红安), and Xiaopeng Jia(贾晓鹏)

Citation: Chin. Phys. B, 2021, 30 (**1**): 016202. DOI: 10.1088/1674-1056/abc4dd
Journal homepage: http://cpb.iphy.ac.cn; http://iopscience.iop.org/cpb

What follows is a list of articles you may be interested in

Nonperturbative effects of attraction on dynamical behaviors of glass-forming liquids

Xiaoyan Sun(孙晓燕), Haibo Zhang(张海波), Lijin Wang(王利近), Zexin Zhang(张泽新), and Yuqiang Ma(马余强)\ccclink

Chin. Phys. B, 2020, 29 (**12**): 126201. DOI: 10.1088/1674-1056/abbbdd

Synthesis of black phosphorus structured polymeric nitrogen

Ying Liu(刘影), Haipeng Su(苏海鹏), Caoping Niu(牛草萍), Xianlong Wang(王贤龙), Junran Zhang(张俊然), Zhongxue Ge(葛忠学), Yanchun Li(李延春)

Chin. Phys. B, 2020, 29 (**10**): 106201. DOI: 10.1088/1674-1056/aba9bd

Nanosheet-structured B_4C with high hardness up to 42 GPa

Chang-Chun Wang(王常春), Le-Le Song(宋乐乐)

Chin. Phys. B, 2019, 28 (**6**): 066201. DOI: 10.1088/1674-1056/28/6/066201

Exploring the compression behavior of HP-$BiNbO_4$ under high pressure

Yin-Juan Liu(刘银娟), Jia-Wei Zhang(张佳威), Duan-Wei He(贺端威), Chao Xu(许超), Qi-Wei Hu(胡启威), Lei Qi(戚磊), A-Kun Liang(梁阿坤)

Chin. Phys. B, 2017, 26 (**11**): 116202. DOI: 10.1088/1674-1056/26/11/116202

High-pressure Raman study of MgV_2O_6 synthesized at high pressure and high temperature

Tang Rui-Lian, Li Yan, Tao Qiang, Li Na-Na, Li Hui, Han Dan-Dan, Zhu Pin-Wen, Wang Xin

Chin. Phys. B, 2013, 22 (**6**): 066202. DOI: 10.1088/1674-1056/22/6/066202

Utilizing of high-pressure high-temperature synthesis to enhance the thermoelectric properties of $Zn_{0.98}Al_{0.02}O$ with excellent electrical properties*

Qi Chen(陈启)[1], Xinjian Li(李欣健)[1], Yao Wang(王遥)[1], Lijie Chang(常立杰)[1], Jian Wang(王健)[1], Yuewen Zhang(张跃文)[2,†], Hongan Ma(马红安)[1,‡], and Xiaopeng Jia(贾晓鹏)[1]

[1] *State Key Laboratory of Superhard Materials, College of Physics, Jilin University, Changchun* 130012, *China*

[2] *Key Laboratory of Material Physics of Ministry of Education, School of Physics and Microeletronics, Zhengzhou University, Zhengzhou* 450052, *China*

(Received 10 September 2020; revised manuscript received 19 October 2020; accepted manuscript online 27 October 2020)

The temperature in the high-pressure high-temperature (HPHT) synthesis is optimized to enhance the thermoelectric properties of high-density ZnO ceramic, $Zn_{0.98}Al_{0.02}O$. X-ray diffraction, scanning electron microscopy, and transmission electron microscopy show that HPHT can be utilized to control the crystal structure and relative density of the material. High pressure can be utilized to change the energy band structure of the samples via changing the lattice constant of samples, which decreases the thermal conductivity due to the formation of a multi-scale hierarchical structure and defects. The electrical conductivity of the material reaches 6×10^4 S/m at 373 K, and all doped samples behave as n-type semiconductors. The highest power factor (6.42 $\mu W\cdot cm^{-1}\cdot K^{-2}$) and dimensionless figure of merit ($zT = 0.09$) are obtained when $Zn_{0.98}Al_{0.02}O$ is produced at 973 K using HPHT, which is superior to previously reported power factors for similar materials at the same temperature. Hall measurements indicate a high carrier concentration, which is the reason for the enhanced electrical performance.

Keywords: high pressure and high temperature, ,icrostructure, Al-doped ZnO, thermoelectric

PACS: 62.50.–p, 72.15.Jf, 72.15.Lh **DOI:** 10.1088/1674-1056/abc4dd

1. Introduction

With increasing global attention on energy and environmental issues, thermoelectric materials have attracted extensive attention because they can directly convert waste thermal energy into electrical energy without producing pollution.[1] The core of this technology lies in the choice of thermoelectric materials, which are strong lightweight materials that do not release harmful gases during utilizing. Some traditional thermoelectric materials contain intermetallic compounds such as Bi_2Te_3 and PbTe, and have shown improved thermoelectric properties.[2–5] However, they are also toxic, expensive, and thermally unstable. In recent years, oxide-based thermoelectric materials have been investigated because most traditional thermoelectric materials are easily oxidized and fail at high-temperatures ($\geq$ 800 K). Zinc oxides are abundant, inexpensive, and environmentally friendly materials that have been investigated as alternative thermoelectric materials for high-temperature applications because of their excellent thermal and chemical stability in air.[6]

The performance of thermoelectric materials is measured by the dimensionless figure of merit, $zT = S^2\sigma T/\kappa$, where S is the Seebeck coefficient, σ is the electrical conductivity, T is the absolute temperature, and κ is the thermal conductivity. High-performance thermoelectric materials have a high power factor ($S^2\sigma$) and low thermal conductivity (κ).[7,8] However, these parameters are closely related to each other so that it is difficult to integrate good electrical properties and low thermal conductivity in a single material.[9,10] This universal principle has become a bottleneck preventing further improvements in thermoelectric materials.

Many studies have focused on decreasing the thermal conductivity of ZnO-based thermoelectric materials,[11,12] while increasing the power factor can also optimize zT values. The thermoelectric material ZnO exhibits a high Seebeck coefficient ($\sim$340 $V\cdot K^{-1}$), whereas its electrical conductivity ($\sim$10 $S\cdot m^{-1}$) is still too low for practical applications.[13] Synthesis at atmospheric pressure is complicated and relatively long and can produce low-density samples, and the donor dopant (such as Al) has limited solubility in ZnO matrixes.[14,15] These factors limit the electrical conductivity and power factor of ZnO-based thermoelectric materials. High-pressure high-temperature (HPHT) methods can accelerate synthesis by using pressure to improve the solubility of the donor dopant in ZnO and to increase the density of the sample.[16]

Many efforts have been devoted to studying the thermoelectric properties of ZnO.[17,18] Tanaka *et al.* used ZnO ceramics sintered by hot-pressing and obtained a power factor

*Project supported by the National Natural Science Foundation of China (Grant No. 51171070) and the Project of Jilin Science and Technology Development Plan, China (Grant No. 20170101045JC).

†Corresponding author. E-mail: zhangyw@zzu.edu.cn

‡Corresponding author. E-mail: maha@jlu.edu.cn

© 2021 Chinese Physical Society and IOP Publishing Ltd

of 4.5 μW·cm^{-1}·K^{-2} at 900 K.[19] Guilmeau *et al.* sintered Al-doped ZnO in air and obtained a maximum power factor of 4.0 μW·cm^{-1}·K^{-2} at 1000 K.[20] Colder *et al.* synthesized $Zn_{1-x}Ni_xO$ through a liquid route and reached a maximum power factor of 5.6 μW·cm^{-1}·K^{-2} at 900 K.[21] Cai *et al.* synthesized ZnO by sol-gel processing and reached a maximum power factor of 1.0 μW·m^{-1}·K^{-2} at 773 K.[22] The above literature shows that the thermoelectric properties of ZnO are greatly affected by the synthesis conditions, microstructure, and density of the sample.

ZnO has poor electrical conductivity, and increasing its power factor is key to making it an excellent thermoelectric material. The utilizing of high pressures may improve its electrical properties by forming a polycrystalline structure, changing the lattice structure, or increasing the oxygen vacancies.[23] Grain refinement can reduce the thermal conductivity at high pressures. Bulk nanomaterials scatter phonons with short mean free paths but have little effect on long-range phonons. However, multi-scale hierarchical structures can scatter full-spectrum phonons, which reduces the thermal conductivity. At the same time, doping can produce enough inherent defects to improve the electrical and thermal properties of ZnO.

Here, we employ a high-pressure technique to investigate the effect of different synthesis temperatures on the thermoelectric properties, morphologies, and structures of Al-doped ZnO.

2. Materials and methods

Commercially available ZnO (99.99%, 50 nm) and Al_2O_3 (99.99%, 30 nm, α-phase) powders were weighed and mixed in a stoichiometric ratio of $Zn_{0.98}Al_{0.02}O$. The accuracy of the balance was 0.0001 g. The obtained powders were cold-pressed into 10.5×6 mm cylinders and then wrapped in molybdenum foil to prevent contamination. Before synthesis, the cylinders were assembled in chambers. The synthesis was conducted with a large-volume cubic high-pressure apparatus (CHPA, SPD-6×1200) at different synthesis temperatures (973 K, 1023 K, 1073 K, and 1123 K) at the same pressure (3 GPa) for 30 min. The samples obtained at 973 K, 1023 K, 1073 K, and 1123 K were denoted as $Zn_{0.98}Al_{0.02}O$-973, $Zn_{0.98}Al_{0.02}O$-1023, $Zn_{0.98}Al_{0.02}O$-1073, and $Zn_{0.98}Al_{0.02}O$-1123, respectively. Platinum-rhodium thermocouples were placed in the chamber to measure the temperature and changes of resistance in comparison with the standard materials, calibrated with temperature. The chamber was quickly quenched to room temperature at high pressure before unloading the pressure. Figure 1 presents a schematic diagram of the chamber.

The phase structure was measured by an x-ray diffractometry (XRD, Rigaku D/Max 2550V/PC, Japan Cu-$K\alpha$ radiation, $\lambda = 0.15418$ nm) with 2θ range from 30° to 70°. Rietveld refinement was performed on the XRD data to obtain the lattice parameters. The cross-sectional morphologies and detailed microstructures were observed using a field-emission scanning electron microscope (FESEM; JEOL JSM-6700F) and a high-resolution transmission electron microscope (HRTEM; JEOL JEM-2200FS), respectively. The samples in dimensions 3×3×6 mm were cut into two pieces by an STX-202A wire cutter. One piece was measured with a Namicro-Ⅲ L (JouleYacht, China) thermoelectric test system to measure the electrical conductivity σ and Seebeck coefficient from 323 K to 973 K. The other sample was measured with the LFA-427 (Germany, NETZSCH) laser flash method to test the thermal diffusion coefficient κ in the same temperature range. Using the relation $\kappa = \lambda C_p D$ to calculate the thermal conductivity (the heat capacity C_p of the sample was calculated by the Dulong–Petit law, and the sample density D was measured by an AE124J electronic balance via Archimedes' principle). All the samples were measured by an HMS-5500 (Hall Effect Measurement System) to determine the Hall coefficient R_H, carrier concentration n, and carrier mobility μ.

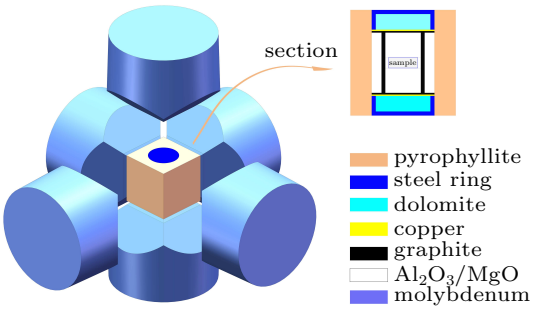


Fig. 1. Schematic of HPHT reactive sintering chamber for $Zn_{0.98}Al_{0.02}O$.

3. Analysis and discussion

We compared the electrical conductivity of ZnO and $Zn_{0.98}Al_{0.02}O$ obtained using the same synthesis parameters (Fig. 2) and found that Al-doped ZnO shows a much higher electrical conductivity because the Al dopant produces electrons via the following reaction:[14,24]

$$Al_2O_3 \xrightarrow{ZnO} 2Al_{Zn}^{\bullet} + 2e' + 2O_O^X + \frac{1}{2}O_2. \quad (1)$$

Oxygen vacancies produced during high-temperature sintering may have acted as donors that produced additional electrons. Increasing the temperature also increases the point defect concentration, according to the equation:[25]

$$c = N_{sites} \exp\left(-\frac{E^f}{k_B T}\right), \quad (2)$$

where c is the point defect concentration, N_{sites} is the number of sites available for defect formation, E^f is the defect formation energy, k_B is Boltzmann's constant, and T is the temperature. The concentration of oxygen vacancies will increase with the temperature, contributed to increasing the overall electrical conductivity.

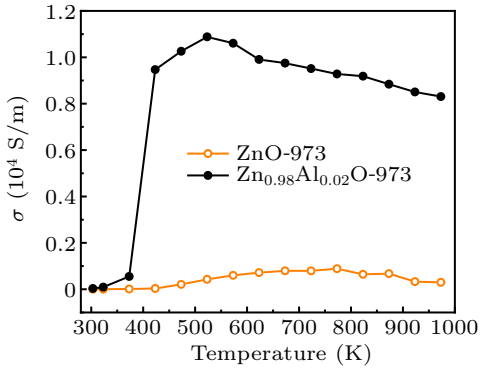


Fig. 2. The electrical conductivity of $Zn_{0.98}Al_{0.02}O$ and ZnO sintered at 973 K.

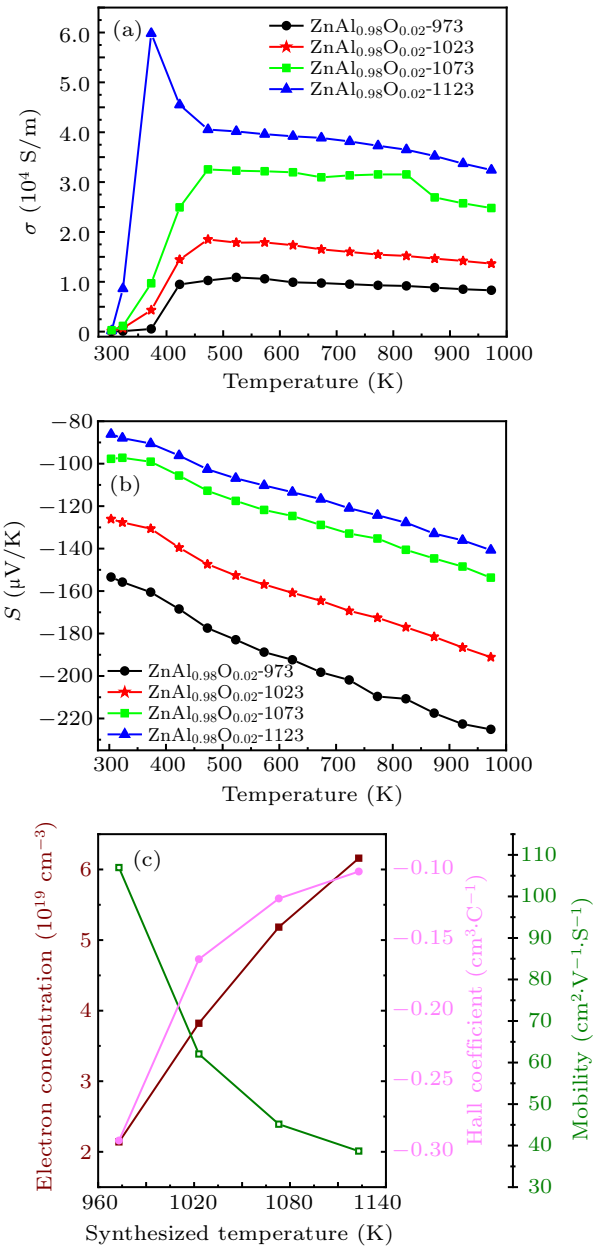


Fig. 3. Temperature dependences of the (a) electrical conductivity and (b) Seebeck coefficient of samples obtained at different synthesis temperatures. HPHT sintering temperature effect on the (c) Hall coefficient R_H, carrier concentration n, and carrier mobility μ of $Zn_{0.98}Al_{0.02}O$ synthesized at different synthesis temperatures.

Figure 3 shows the changes in the electrical properties of the samples with temperature. Figure 3(a) illustrates that the electrical conductivity increases with the temperature before beginning to slowly decrease. At about 453 K, the electrical conductivity of the samples sharply increases. The sample shows metallic behavior at test temperatures higher than 500 K, which is consistent with the previously reported trends. We speculate that this change may arise from the modulation of energy bands by high pressure and high temperature.[26] The electrical conductivity of all the samples reaches a maximum between 400 K and 500 K, and the highest electrical conductivity is obtained in the sample synthesized at 1123 K. At 373 K, the electrical conductivity of $Zn_{0.98}Al_{0.02}O$-1123 increases from 552 S/m to 6×10^4 S/m as the sintering temperature increases. Figure 3(b) shows that the absolute value of the Seebeck coefficient gradually increases with the test temperature. The Seebeck coefficients of all the samples are negative, which shows that electrical transmission proceeds mainly via electron conduction. At the same test temperature, the absolute value of the Seebeck coefficient decreases at higher sintering temperatures. In addition, Hall measurement was conducted to understand the carrier transport. Figure 3(c) shows that increasing the sintering temperature will increase oxygen deficiency (the carrier concentration of $Zn_{0.98}Al_{0.02}O$-1123 reaches 6.16×10^{19} cm^{-3}).

Figure 4 shows that the power factor of $Zn_{0.98}Al_{0.02}O$-1123 increases significantly with the test temperature, and a maximum power factor of 6.42 $\mu W\cdot cm^{-1}\cdot K^{-2}$ is obtained at 973 K. The power factor does not appear to be saturated, suggesting that it can continue to increase at temperatures higher than 1000 K.

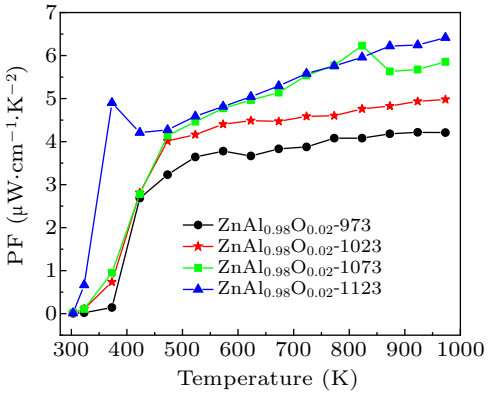


Fig. 4. Temperature dependence of the power factor during the optimization of HPHT temperature.

Figure 5(a) presents the temperature dependences of the sample's total thermal conductivity (κ_{tot}), which is contributed by both the electronic thermal conductivity κ_e and the lattice thermal conductivity κ_{lat}, where κ_e is proportional to the electrical conductivity, $\kappa_e = \sigma LT$ (the Wiedemann–Franz law). Here, L is the Lorentz number (2.45×10^{-8} $V^2\cdot K^{-2}$).[27] Subtracting κ_e from κ_{tot} we obtain κ_{lat}, as plotted in Fig. 5(b). The

results show that the total thermal conductivity κ_{tot} and lattice thermal conductivity κ_{lat} of the sample remain small as the HPHT sintering temperature increases.

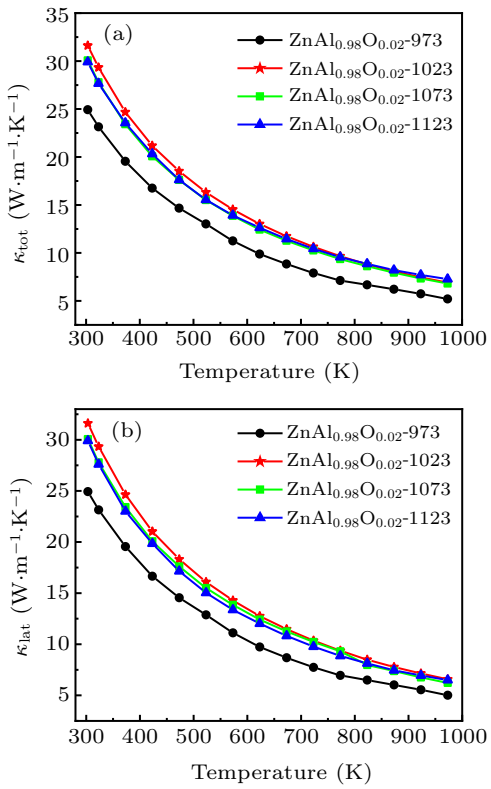


Fig. 5. (a) Total thermal conductivity and (b) lattice thermal conductivity of $Zn_{0.98}Al_{0.02}O$ versus temperature.

The electrical and thermal properties of zinc oxide thermoelectric materials can be optimized by adjusting the pressure and temperature during HPHT. The dimensionless figures of merit of our samples as a function of temperature, zT, are depicted in Fig. 6. Here zT greatly increases as the electrical performance of zinc oxide is improved, whereas zT does not appear to become saturated as the test temperature increases, suggesting that zT will continue to increase above 1000 K. In general, the zT value increases with the sintering temperature, showing that the HPHT sintering temperature plays a dominant role in the thermoelectric performance of the sample.

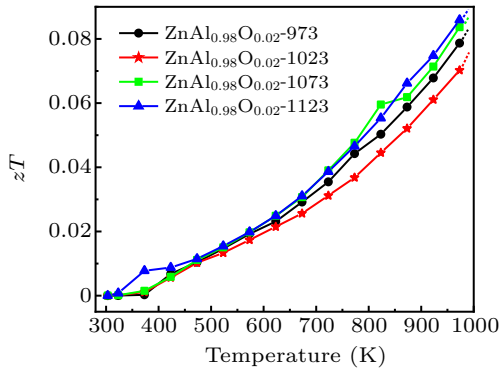


Fig. 6. Temperature dependences of the zT values of $Zn_{0.98}Al_{0.02}O$.

3.1. Relative density and band structure

Figure 7 shows the XRD pattern of the sample optimized by HPHT. No impurity peaks were detected in the XRD pattern, indicating that Al was completely doped into ZnO. It is also shown that HPHT improved the solubility of Al in ZnO.[28] Within the range of 2θ (30°–70°), the peak positions of all the samples are consistent with hexagonal ZnO (space group $P63mc$, PDF No. 80-75). This indicates that hexagonal ZnO was sintered within 30 min (the structure model of ZnO on the left side of the label in Fig. 7). Conventional synthesis methods often require more than 12 hours, which means that the utilizing of a high pressure greatly improved the synthesis efficiency. The peak intensity of the XRD pattern gradually increases with the synthesis temperature. It can be inferred that high temperature can promote the synthesis of $Zn_{0.98}Al_{0.02}O$.

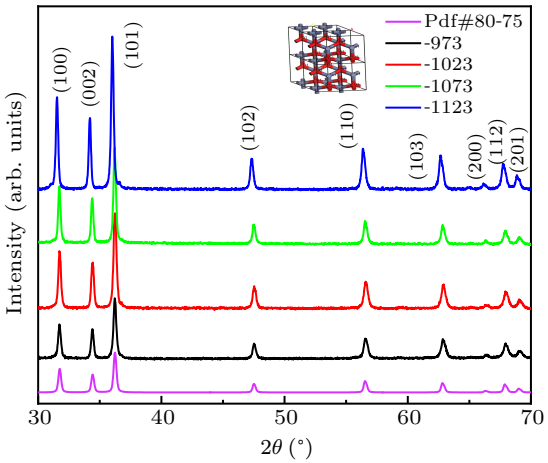


Fig. 7. XRD patterns of $Zn_{0.98}Al_{0.02}O$ synthesized at 3 GPa and at different temperatures.

To study the effect of the synthesis temperature under high pressure on the relative density of $Zn_{0.98}Al_{0.02}O$, we obtained the Rietveld structural refinement from the XRD data using GSAS (general structure analysis system). Figure 8(a) shows the refined curves of the sample synthesized at 1123 K and 3 GPa. The lattice constants of the sample synthesized at 3 GPa were obtained from the refined results ($a = b = 3.245$ Å; $c = 5.198$ Å). The lattice structure of ZnO was changed (ambient pressure $a = b = 3.25$ Å; $c = 5.2$ Å). All other samples were refined in the same way, and the XRD refinement results were inserted into the following formula to calculate the theoretical density (TD):[29]

$$\mathrm{TD} = \frac{M_{Zn_{0.98}Al_{0.02}O}}{V_{unit} \times N_A}, \tag{3}$$

where $M_{Zn_{0.98}Al_{0.02}O}$ is the relative molecular mass of $Zn_{0.98}Al_{0.02}O$, V_{unit} is the unit cell volume of the sample, and N_A is Avogadro's number. Archimedes' principle was used to obtain the true density of the sample (ρ). Figure 8(b) shows that the relative density (RD) of the samples (RD = ρ/TD) increases at higher sintering temperatures.[30,31]

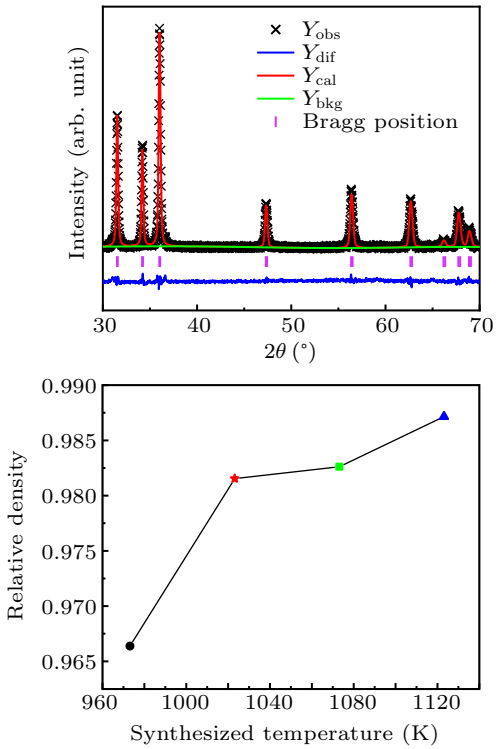


Fig. 8. (a) X-ray Rietveld refinement profile of $Zn_{0.98}Al_{0.02}O$ synthesized at 1123 K. (b) Relative density of samples at different synthesis temperatures.

The refinement results were used to calculate the band structures using CASTEP software package. The band gap was underestimated using density functional theory (local density approximation). We found that the energy band structure at high pressure underwent tremendous changes (ambient pressure band gap = 3.2 eV), possibly due to changes in its lattice structure. The band structure details at 3 GPa are shown in Fig. 9, and the results at different pressures show a similar trend. Both the conduction band minimum (CBM) and the valence band maximum (VBM) are located at vector ***G*** in Fig. 9, which means that ZnO synthesized at high pressures (3 GPa) is a direct band gap semiconductor.[32]

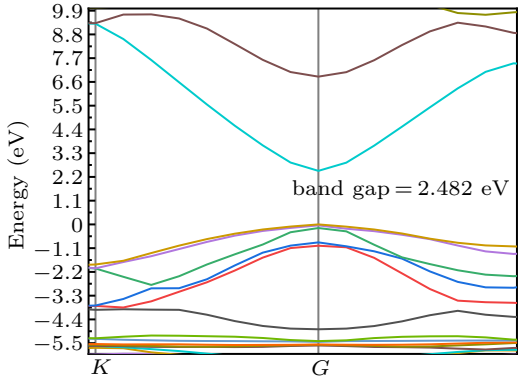


Fig. 9. Band structure at 3 GPa.

3.2. Microstructure and morphological characterization

To optimize the HPHT temperature and determine its effects on the micro morphology (Fig. 10) of the samples, the fracture surfaces of the samples were characterized by scanning electron microscopy (SEM). Figures 10(a)–10(d) give the low-magnification SEM images showing the sample morphologies. Regardless of the sintering temperature, all the samples were covered with deposits of various sizes, which decrease the thermal conductivity. From Figs. 10(a)–10(d), the grain size generally coarsens, and the crystallinity of the sample is improved at higher synthesis temperatures, with increasingly fewer pores between grains. Figures 10(e)–10(h) show the high-magnification SEM images of the sample morphologies. Nanoscale grains of various sizes are randomly distributed between the sample surface and the crystal surface due to grain refinement at 3 GPa.

HPHT synthesis methods provide more freedom for adjusting the synthesis pressure, which can be used to tune the thermoelectric properties of a material.[33] The micromorphologies of samples synthesized using HPHT change at different temperatures, and the ideal ZnO morphology could be obtained by changing the pressure and temperature during HPHT synthesis.

The micromorphology of $Zn_{0.98}Al_{0.02}O$-1123 was characterized by TEM (Fig. 11). Figure 11(a) shows fringes (black areas), along with particles of various shapes and sizes. Figure 11(d) presents the medium-magnification TEM image, which also shows fringes in the sample. Figure 11(f) gives the localized electron diffraction pattern of the yellow rectangular frame in Fig. 11(d) and shows that HPHT is useful for manufacturing polycrystalline structures. Figure 11(b) shows the presence of many lattice defects (white circles) and dislocations (red circles). The small image on the upper left of Fig. 11(b) is the IFFT transform of the red area, which makes changes in the fringes more obvious. Figures 11(c) and 11(e) show many lattice defects (white circles) and crystal shear defects (green circles). The small graph on the upper left of Fig. 11(c) is the FFT of the white circle area. The distribution of the frequency domain corresponding to defects is helpful for analyzing the defects. Figures 11(b), 11(c), and 11(e) contain fringes with different pitches. These fringes belong to the (102) crystal plane detected by XRD. The slight change in the interplanar spacing is caused by the application of a pressure of 3 GPa.

The utilizing of high pressure can form many lattice defects, and high-pressure quenching promotes the growth of nanoscale grains. The defects improve the thermoelectric properties of the material, suggesting that HPHT can be used to obtain desired morphologies.[34]

The HPHT sintering temperature greatly affects the electrical properties of $Zn_{0.98}Al_{0.02}O$, showing that the electrical properties of the sample are improved due to changes in the microstructure and morphology of the material.

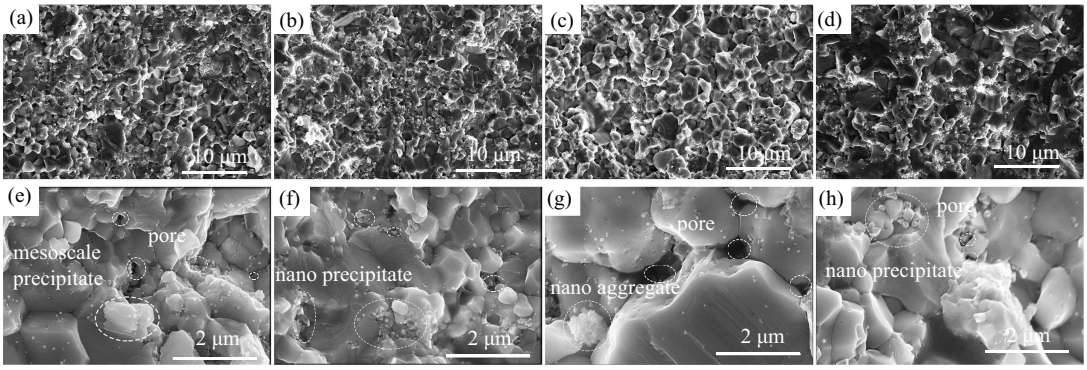


Fig. 10. (a)–(d) Low-magnification SEM images of the sample morphologies used to optimize the temperature during HPHT synthesis and (e)–(h) high-magnification SEM images of the same samples: (a) and (e) $Zn_{0.98}Al_{0.02}O$-973; (b) and (f) $Zn_{0.98}Al_{0.02}O$-1023; (c) and (g) $Zn_{0.98}Al_{0.02}O$-1073; (d) and (h) $Zn_{0.98}Al_{0.02}O$-1123.

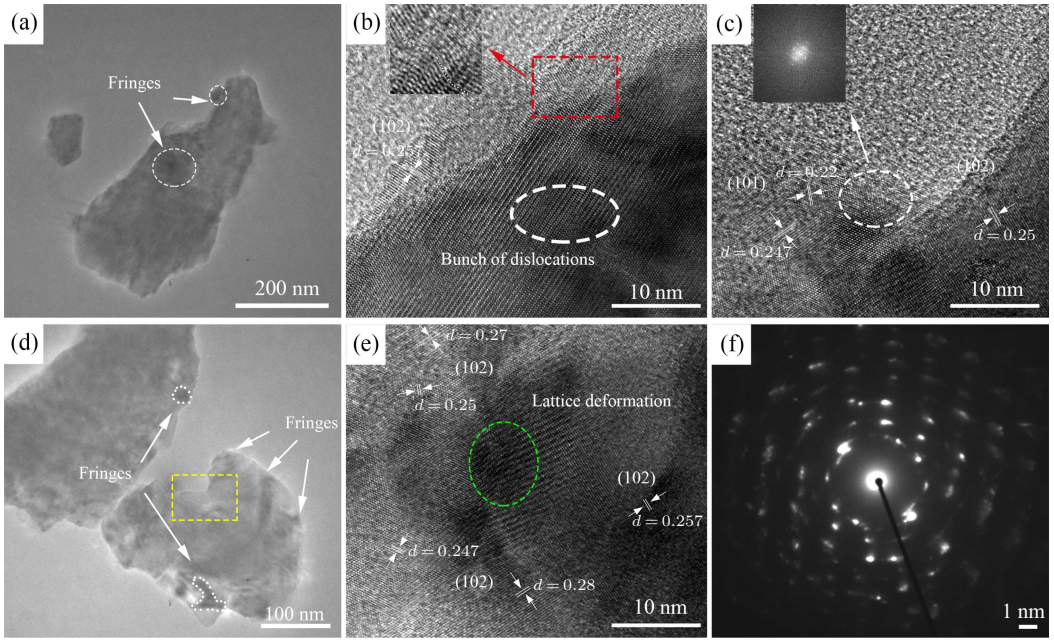


Fig. 11. (a) and (d) Low-magnification TEM images taken from a representative $Zn_{0.98}Al_{0.02}O$-1123 sample; (b), (c) and (e) HRTEM images of this sample showing the presence of multiple microstructures; (f) the electron diffraction pattern of the yellow selection in (d).

In conventionally sintered thermoelectric materials, the thermal conductivity increases at higher temperatures, which does not help increase the zT of thermoelectric materials because the relative density decreases at higher synthesis temperatures. Although the thermal conductivity of a sample can be effectively reduced at lower densities, the electrical properties are also greatly reduced. However, the utilizing of HPHT increases the degrees of freedom of the pressure compared with conventional methods, allowing the electrical and thermal properties of thermoelectric materials to be adjusted.

The thermal conductivity of the sample decreases monotonously as the test temperature increases, possibly due to grain refinement at a high pressure.

There is a well-known relationship between phonon relaxation time τ and lattice thermal conductivity $\kappa_{\rm lat}$

$$\kappa_{\rm lat} = \frac{1}{3} C_{\rm V} v l = \frac{1}{3} C_V v^2 \tau, \tag{4}$$

where $C_{\rm V}$, v, and l are the constant-volume specific heat, phonon velocity, and phonon mean-free path, respectively.[35] For a particular material, $C_{\rm V}$ and v are different. The relaxation time of phonon scattering can be written as

$$\tau^{-1} = \tau_{\rm p}^{-1} + \tau_{\rm n}^{-1} + \tau_{\rm me}^{-1} + \tau_{\rm mi}^{-1} + \tau_{\rm u}^{-1}, \tag{5}$$

where $\tau_{\rm p}$, $\tau_{\rm n}$, $\tau_{\rm me}$, $\tau_{\rm mi}$, and $\tau_{\rm u}$ are the relaxation times corresponding to point defect phonon scattering, nanoscale scattering agents, mesoscale scattering agents, micrometer-scale grain boundaries, and Umklapp scattering, respectively.[36]

The XRD data show that HPHT changes the ZnO lattice structure, and the SEM and TEM images show that HPHT makes a multi-scale hierarchical structure form and defects serve as phonon scattering sources. Phonon scattering mechanisms are affected by the size scale of the media,[36] but all size scales can hinder phonon propagation and increase scattering. The samples exhibit low thermal conductivity because the multi-scale hierarchical structure induces full-spectrum phonons scattering. Finally, the phonon propagation in samples obtained at high temperatures is dominated by high-frequency phonons with short and medium length scales. The

shorter lattice thermal conductivity at a high temperature occurs mainly because of high-frequency phonons scattering by point defects and Umklapp scattering. Increasing the test temperature enhances all scattering effects, which explains why the lattice thermal conductivity of our samples decreases at higher test temperatures.

4. Conclusion

To improve the electrical properties of ZnO while maintaining a low thermal conductivity, the temperature in the HPHT synthesis is optimized. As the synthesis temperature increases at 3 GPa, the band gap of ZnO greatly decreases, and its microporosity gradually decreases. HPHT increases the electrical conductivity of $Zn_{0.98}Al_{0.02}O$ to 6×10^4 S/m at 373 K, and its power factor increases to 6.42 $\mu W\cdot cm^{-1}\cdot K^{-2}$ at 973 K. The electrical properties are greatly improved because HPHT changes the band structure and increases the relative density of the zinc oxide. Grain refinement and the production of a multi-scale hierarchical structure at high pressure are the main factors for retaining zinc oxide's low thermal conductivity. Finally, improved zT values (0.09 at 973 K) are obtained in $Zn_{0.98}Al_{0.02}O$-1123.

References

[1] Minnich A J, Dresselhaus M S, Ren Z F and Chen G 2009 *Energy & Environ. Sci.* **2** 466

[2] Poudel B, Hao Q, Ma Y, Lan Y, Minnich A, Yu B, Yan X, Wang D, Muto A, Vashaee D, Chen X, Liu J, Dresselhaus M S, Chen G and Ren Z 2008 *Science* **320** 634

[3] Pei Y, LaLonde A D, Heinz N A, Shi X, Iwanaga S, Wang H, Chen L and Snyder G J 2011 *Adv. Mater.* **23** 5674

[4] Madavali B, Kim H S, Lee K H, Isoda Y, Gascoin F and Hong S J 2016 *Mater. & Design* **112** 485

[5] Feng S K, Li S M and Fu H Z 2014 *Chin. Phys. B* **23** 117202

[6] Cheng P, Song J, Li S, Li J and Wang C 2015 *IEEE 11th International Conference on the Properties and Applications of Dielectric Materials (ICPADM)*, 19–22 July 2015, Sydney, NSW, Australia, pp. 212–215

[7] Wei J, Yang L, Ma Z, Song P, Zhang M, Ma J, Yang F and Wang X 2020 *J. Mater. Sci.* **55** 12642

[8] Liu H Q, Zhao X B, Liu F, Song Y, Sun Q, Zhu T J and Wang F P 2008 *J. Mater. Sci.* **43** 6933

[9] Tan G, Zhao L D and Kanatzidis M G 2016 *Chem. Rev.* **116** 12123

[10] Snyder G J and Toberer E S 2008 *Nat. Mater.* **7** 105

[11] Jood P, Mehta R J, Zhang Y, Peleckis G, Wang X, Siegel R W, Borca-Tasciuc T, Dou S X and Ramanath G 2011 *Nano Lett.* **11** 4337

[12] Gautam D, Engenhorst M, Schilling C, Schierning G, Schmechel R and Winterer M 2015 *J. Mater. Chem. A* **3** 189

[13] Tsubota T, Ohtaki M, Eguchi K and Arai H 1997 *J. Mater. Chem.* **7** 85

[14] Hoemke J, Khan A U, Yoshida H, Mori T, Tochigi E, Shibata N, Ikuhara Y and Sakka Y 2016 *J. Ceram. Soc. Jpn.* **124** 515

[15] Kinemuchi Y, Nakano H, Mikami M, Kobayashi K, Watari K and Hotta Y 2010 *J. Appl. Phys.* **108** 053721

[16] Zhu P W, Jia X, Chen H Y, Guo W L, Chen L X, Li D M, Ma H A, Ren G Z and Zou G T 2002 *Solid State Commun.* **123** 43

[17] Ohtaki M and Araki K 2011 *J. Ceram. Soc. Jpn.* **119** 813

[18] Ohtaki M, Araki K and Yamamoto K 2009 *J. Electron. Mater.* **38** 1234

[19] Tanaka Y, Ifuku T, Tsuchida K and Kato A 1997 *J. Mater. Sci. Lett.* **16** 155

[20] Guilmeau E, Maignan A and Martin C 2009 *J. Electron. Mater.* **38** 1104

[21] Colder H, Guilmeau E, Harnois C, Marinel S, Retoux R and Savary E 2011 *J. Eur. Ceram. Soc.* **31** 2957

[22] Cai K F, Müller E, Drašar C and Mrotzek A 2003 *Mater. Sci. Engin. B* **104** 45

[23] Liu H, Ma H, Zhang Y, Sun B, Liu B, Kong L, Liu B and Jia X 2017 *Inorg. Chem.* **56** 11275

[24] Bai Y, Zhao J, Lv Z and Lu K 2020 *J. Mater. Sci.* **55** 14112

[25] Ong K P, Singh D J and Wu P 2011 *Phys. Rev. B* **83** 115110

[26] Liu H, Ma H, Wang C, Wang F, Liu B, Chen J, Ji G, Zhang Y and Jia X 2018 *Ceram. Int.* **44** 19859

[27] Walia S, Balendhran S, Nili H, Zhuiykov S, Rosengarten G, Wang Q H, Bhaskaran M, Sriram S, Strano M S and Kalantar-Zadeh K 2013 *Prog. Mater. Sci.* **58** 1443

[28] Bérardan David, Byl Céline, Dragoe Nita 2010 *J. Am. Ceram. Soc.* **93** 2352

[29] Rosten R, Koski M and Koppana E 2006 *J. Undergrad. Mater. Res.* **2** 38

[30] Hng H H and Tse K Y 2003 *J. Mater. Sci.* **38** 2367

[31] Fan J and Freer R 1997 *J. Mater. Sci.* **32** 415

[32] Li P, Deng S H, Zhang L, Yu J Y and Liu G H 2010 *Chin. Phys. B* **19** 117102

[33] Zhu H, Su T, Li H, Pu C, Zhou D, Zhu P and Wang X 2017 *J. Eur. Ceram. Soc.* **37** 1541

[34] Sun B, Jia X, Zhao J, Li Y, Liu H and Ma H 2018 *Inorg. Chem.* **57** 3323

[35] Zhang Y, Jia X, Sun H, Sun B, Liu B, Liu H, Kong L and Ma H 2016 *J. Materiomics* **2** 316

[36] Luo Y, Jiang Q, Yang J, Li W, Zhang D, Zhou Z, Cheng Y, Ren Y, He X and Li X 2017 *Nano Energy* **32** 80